

Aggregation-induced emission enhancement characteristics of naphthalimide derivatives and their applications in cell imaging†

Hsin-Hung Lin,^a Yung-Chieh Chan,^b Jyun-Wei Chen^a and Cheng-Chung Chang^{*a}

Received 4th September 2010, Accepted 3rd December 2010

DOI: 10.1039/c0jm02942d

Novel naphthalimide derivatives (NIM) with donor–acceptor architecture were successfully constructed and their unique fluorescent properties were investigated. In particular, the fluorescence intensities of 4-methoxystyrene substituted **NIM-1** were solvent independent and its quantum yields varied from 0.4 in toluene to 0.52 in MeOH. However, 4-(*N,N*-diphenylamino) styrene substituted **NIM-2** and 4-nitrostyrene substituted **NIM-3** exhibited low luminescence in dilute solutions but were efficiently fluorescent under conditions of molecular aggregation. **NIM-2** showed strong solid fluorescence with a longer wavelength emission and larger Stokes shift. In addition, **NIM-3** showed unexpected blue-green fluorescence due to the formation of fluorescent organic nanoparticles (FONs) under mixed solution. These two cases were ascribed to the aggregation-induced enhanced emission (AIEE) effects and which can also reasonably explain the bright cellular images observed when cells were incubated with **NIM-2** and **NIM-3**. Furthermore, compound **NIM-2** can be used to recognize cancer cells owing to its subcellular behaviour.

Introduction

Fluorescent dyes have specialized applications in biodiagnostic assays.¹ Thus, the development of high-efficiency fluorophores is essential for the field of molecular sensors.² Most conventional fluorophores have the disadvantage of very small Stokes shifts, which can lead to self-quenching and measurement error caused by the excitation light and scattering. High levels of self-quenching can also result in weak solid fluorescence, which might partly explain why aggregation of fluorescent probe is unfavorable for cellular staining. Furthermore, most organic fluorescent dyes exhibit fluorescence quenching in the aggregate or solid states, and this results in the nonradiative deactivation of the excited state becoming dominant because of the formation of delocalized excitons or excimers.³ Recently, organic dyes that exhibit strong fluorescent emission in their aggregate or solid state have attracted increasing attention,⁴ such as siloles,⁵ 1-cyano-*trans*-1,2-bis(4'-methylbiphenyl)ethylene,⁶ thienyl-azulene,⁷ arylolethene derivatives,⁸ 1,4-di[(*E*)-2-phenyl-1-propenyl]benzene,⁹ and salicylaldehyde azine derivatives.¹⁰ These fluorophores show aggregation-induced emission enhancement

(AIEE) characteristics which promote great application potential as well as challenge the current knowledge of the photoluminescence process. Thus, to extend our understanding of fluorescence mechanisms, exploration of new AIEE fluorophores is of great interest.

1,8-Naphthalimide derivatives are a well-known class of compounds that have a wide range of applications. Because of their high fluorescence quantum yields and photostability, these derivatives are considered to be good candidates for fluorescent dichroic dyes,¹¹ fluorescent polymeric paints or plastics¹² and fluorescent markers in medicine and biology.¹³ Moreover, the use of 1,8-naphthalimide derivatives as DNA intercalators¹⁴ and functionalized naphthalimide chromophores have been under examination in solution as sensor dyes for metal ions¹⁵ and for pH-changes.¹⁶ However, a review of previous investigations about the synthesis and properties of 1,8-naphthalimide derivatives revealed that most derivatives have been functionally modified on the basis of the 1,8-naphthalimide structure containing various alkylamino groups in the 4-position or *N*-substitutions of the naphthalimide ring. In addition, their spectral properties result in absorbance at short wavelengths (below 400 nm); this is particularly problematic for biological experiments because operations in the visible range of wavelengths are common-place for biological applications involving aqueous systems. As a result, the choice of functional naphthalimide dyes is much more limited for confocal microscopy systems. In the present study, our intention was to extend the scope of available naphthalimide dyes by elongating the π -conjugate resonance of rings and to describe in more detail about their spectroscopic properties. When electron donor

^aGraduate Institute of Biomedical Engineering, National Chung Hsing University, 250 Kuo Kuang Road, Taichung, 402, Taiwan, R.O.C. E-mail: ccchang555@dragon.nchu.edu.tw; Fax: (+886)-4-228 52422; Tel: (+886)-4-22840734 ext. 24

^bDepartment of Chemistry, National Chung Hsing University, 250 Kuo Kuang Road, Taichung, 402, Taiwan, R.O.C

† Electronic supplementary information (ESI) available: Details of materials synthetic procedures, immunofluorescence staining of **NIM-1**, **NIM-2** and **NIM-3**. See DOI: 10.1039/c0jm02942d

groups were linked to the electron-acceptor naphthalimide core, an intramolecular charge transfer occurred. Furthermore, the new D–A structures were fabricated and the vinyl group worked as a π spacer to link the donor and the acceptor; this extended the conjugation systems to favor absorption and emission.

In previous studies, we described the AIEE properties and developed fluorescent organic nanoparticle (FON) models of anionic and cationic 10*H*-phenothiazine derivatives.^{17,18} In particular, the AIEE properties of protonated phenothiazine were observed for both *in vitro* spectral studies and cellular staining. Then, we developed a vacuole model using FONs to elucidate the formation of fluorescent bright spots that are considered to form in the lysosomes of cancer cells and can be used in cancer cell recognizer fluorophores.¹⁸ In the present study, we present the absorption and photoluminescence features of naphthalimide chromophores substituted with 4-methoxystyrene, 4-(*N,N*-diphenylamino)styrene, 4-nitrostyrene and 4-hydroxystyrene moiety groups. Solvatochromic studies of the different chromophores were performed to determine the changes in dipole moments under excitation and to compare the results with the observed photoluminescence efficiency. Then, the AIEE properties were investigated and these phenomena were applied to illustrate the cellular imaging. Finally, we tested the ability of the chromophores to be used as cellular probes.

Experimental section

1. Materials

The general chemicals employed in this study were of the best grade available and were obtained from Acros Organic Co., Merck Ltd., or Aldrich Chemical Co. and used without further purification. All solvents were of spectrometric grade.

2. Apparatus

Absorption spectra were generated using a *Thermo Genesys 6* UV-visible spectrophotometer, and fluorescence spectra were recorded using a *HORIBA JOBIN-YVON Fluoromas-4* spectrofluorometer with a 1 nm band-pass and a 1 cm cell length at room temperature. Transmission electron microscopy (TEM) was conducted on a *Zeiss EM 902A* operated at 80 kV. A mixed solution (a mixed solvent of THF and deionized water, 75/25 v/v; ref. 26) containing compound **NIM-3** was deposited onto carbon-coated copper grid.

3. Determination of quantum yields

The quantum yields of NIM derivatives were determined as previously described using the following equation:¹⁹

$\Phi_u = \Phi_s \times [A_{fu} \times A_s(\lambda_{exs}) \times \eta_u^2] / [A_{fs} \times A_u(\lambda_{exu}) \times \eta_s^2]$ where Φ_u is the quantum yield of unknown; A_f is the integrated area under the corrected emission spectra; $A(\lambda_{ex})$ is the absorbance area at the excitation wavelength; η is the refractive index of the solution; the subscripts u and s refer to the unknown and the standard, respectively. For the same λ_{ex} , we chose 3,6-bis-(1-methyl-4-vinylpyridinium)carbazole diiodide (BMVC) as the standard, which has a quantum yield of 0.25 in glycerol and 0.02 in DMSO.²⁰

4. Cell culture conditions and compound incubation

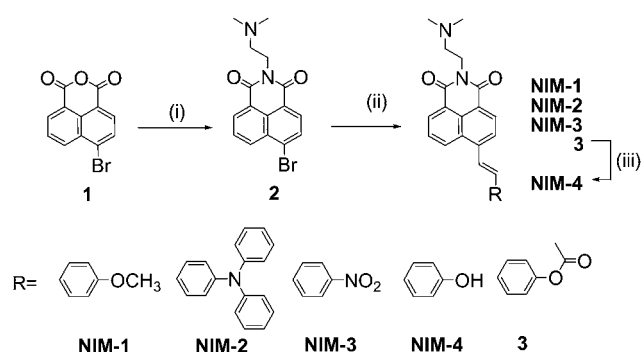
The human embryonal lung MRC-5 normal fibroblast cells and MCF7 human breast cancer cell were grown in Dulbecco's modified Eagle's medium (DMEM) with non-essential amino acids supplemented with 10% fetal calf serum (FCS). The human lung adenocarcinoma cell lines CL1-0 cancer line were grown in RPMI 1640 (Gibco/Invitrogen™, Cat. no. 22400-089) medium containing 10% fetal bovine serum (FBS). Cell cultures were maintained at 37 °C in a humidified atmosphere of 95% air and 5% CO₂. The cells seeded in culture plates or dishes were incubated with different concentrations of NIM derivatives, whose DMSO stock solutions were diluted in serum-free medium before use (1/100 v/v).

5. Cellular imaging

Before the observation of cellular localization, cells were seeded into coverslips and incubated for 24 h. On the next day, cells were incubated with 10 μ M of NIM for 4 h, and then the fluorescence images were taken under *Leica AF6000* confocal fluorescence microscopy with DFC310 FX Digital color camera; or the λ scanning and fluorescence images were taken under *Leica TCS SP5* confocal fluorescence microscopy. The excitation source was a 405 nm diode laser for compounds. Fluorescence photographs were taken through related ranges by photomultiplier tubes (PMT).

6. General procedure for the synthesis of naphthalimide derivatives

Synthesis of the naphthalimide derivatives is shown in Scheme 1. The first stage of the reaction, in which commercial starting material 4-bromo-1,8-naphthalic anhydride was reacted with the RNH₂, was performed conveniently in ethanol at room temperature. Next, the samples were subjected to the Heck coupling reaction with 4-methoxystyrene, 4-*N,N*-diphenylaminostyrene, 4-nitrostyrene or 4-acetoxystyrene under catalyst Pd(OAc)₂.²¹ Details of materials synthetic procedures and identifications are shown in the Supporting Information.† **NIM-1**: 2-(6-(4-methoxystyryl)-1,3-dioxo-1*H*-benzo[de]isoquinolin-2(3*H*)-yl)-*N,N*-dimethylethanamine. **NIM-2**: 2-(6-(*N,N*-diphenyl-4-



Scheme 1 Reagents and conditions: (i) *N,N*-dimethylethane-1,2-diamine, EtOH, r.t. 24 h; (ii) Pd(OAc)₂/(*o*-tol)₃P, 4-methoxystyrene (**NIM-1**), 4-(*N,N*-diphenylamino)styrene (**NIM-2**), 4-nitrostyrene (**NIM-3**), or 4-acetoxystyrene (compound 3), Et₃N/MeCN, N₂, reflux, 48 h. (iii) KOH/MeOH, reflux, 2 h; then HCl.

aminostyryl)-1,3-dioxo-1H-benzo[de]isoquinolin-2(3H)-yl)-*N,N*-dimethylethanamine. **NIM-3**: 2-(6-(4-nitrostyryl)-1,3-dioxo-1H-benzo[de]isoquinolin-2(3H)-yl)-*N,N*-dimethylethanamine. **NIM-4**: 2-(6-(4-hydroxystyryl)-1,3-dioxo-1H-benzo[de]isoquinolin-2(3H)-yl)-*N,N*-dimethylethanamine.

Molecular design and synthesis

Ethylene acts as the π -linker at the centre of the D- π -A type chromophore structure. In this investigation, the naphthalimide moiety was selected as the π -electron acceptor because of its good chemical stability and the commercial availability of various useful molecular building blocks. The 4-methoxyphenyl, triphenylamine, and 4-hydroxyphenyl moieties were chosen as the electron-donating unit (molecules **NIM-1**, **2**, and **4**). Alternatively, the 4-nitrophenyl moiety was used as electron-acceptor in molecule **NIM-3** to construct an A- π -A type chromophore and its fluorescence properties with respect to other naphthalimide derivatives were investigated. Next, to avoid decomposition of the naphthalic anhydride upon Heck reaction, 4-bromo-1,8-naphthalic anhydride, the starting material, was reacted with *N,N*-dimethylethylenediamine in ethanol as the initial reaction step. We also examined this imidation reaction under other reaction conditions such as 1,4-dioxane, tetrahydrofuran, ethanol and dimethylformamide for an appropriate refluxing time period.²² However, the expected amine containing imide substituent was not obtained because amination also occurred on the 4-position with Br. Moreover, we propose that the spacer *N,N*-dimethylethylenediamine should be more suitable than other aliphatic chains in cellular staining. Finally, the naphthalimide derivative was coupled with aryl olefins. That is, the vinyl aryl substituents—either electron donor or acceptor—were substituted at the 4-positions of naphthalimide and the molecular structures of the compounds were shown in Scheme 1.

Basic spectroscopic properties

The wavelengths of maximum absorption and emission, molar absorptivity, quantum yields and Stokes shifts of the all new NIM compounds in different organic solvents comparing a wide polarity range are listed in Table 1. No significant solvent polarity dependent spectral shifts in the absorption spectra were observed for any of the dyes. This indicates that, in their ground

states, these chromophores are not significantly stabilized by solvation due to a relatively small dipole moment. Conversely, as shown in Fig. 1, strong solvatochromic red shifts of the emission spectra were observed for compounds **NIM-1**, **NIM-2** and **NIM-4** with increasing solvent polarity. Therefore, the maximum red shifts observed in the emission spectra when increasing the polarity were 88 nm, 122 nm, 52 nm and 90 nm for **NIM-1**, **NIM-2**, **NIM-3** and **NIM-4**, respectively. When comparing the fluorescence properties of these chromophores, **NIM-2** showed longer emission wavelengths in all investigated solvents, as well as the largest Stokes shifts. This was likely because the auxiliary electron-donating ability of triphenylamine units offered good effective conjugation in the π -linked donor compounds and increased fluorescent solvatochromism. Alternatively, the absorption bands of the **NIM-3** were blue shifted and lower than 400 nm which can be attributed to the electron withdrawing group of nitrobenzyl at the 4-position of naphthalimide core.

Further information regarding the solvent sensitivity of the absorption and emission spectra of these dyes was obtained from evaluation of the Stokes shifts of each of the NIM dyes in terms of Lippert plots.²³ The Lippert-Mataga equation describes the dependence of the energy difference between the ground state and the excited state (in cm^{-1}) on the refractive index (n) and the dielectric constant (ϵ) of the solvent:

$$\begin{aligned} \nu_A - \nu_F &= 2/hc \times \Delta\mu^2 \times \Delta f \times a^{-3} + \text{constant} \\ \Delta f &= (\epsilon - 1)/(2\epsilon + 1) - (n^2 - 1)/(2n^2 + 1), \quad \Delta\mu = \mu_E - \mu_G \\ (\nu_A - \nu_F)/\Delta f &= 11307.6 \Delta\mu^2 \times a^{-3} + \text{constant} \end{aligned}$$

where ν_A and ν_F are the wavenumbers (cm^{-1}) of the absorption and emission maxima, respectively. $h = 6.6256 \times 10^{-27}$ erg s is Planck's constant; $c = 2.9979 \times 10^{10}$ cm s^{-1} is the speed of light; and a is the radius of the cavity in which the fluorophore resides; μ_G and μ_E refer to the ground state and excited state dipole moments, respectively; and the term Δf is the orientation polarizability. The slope of the Lippert plot reflects the solvent sensitivity of a fluorophore. The calculated values of Δf for each solvent are presented in Table 1 and the plot of $\Delta\nu$ ($\nu_A - \nu_F$) vs. Δf , for these solvents we examined, is presented in Fig. 2a. Positive solvatochromism was found for all chromophores, indicating that the involvement of solvent polarity dependent intramolecular charge transfer (ICT) emissive states.²⁴ In addition, a degree of deviation from

Table 1 Photophysical data of **NIM-1** to **NIM-4** in solvents of different polarities.^a

Solvent (Δf)	NIM-1			NIM-2			NIM-3			NIM-4		
	λ_{abs} (ϵ)	λ_{em} (Φ)	$\Delta\nu$	λ_{abs} (ϵ)	λ_{em} (Φ)	$\Delta\nu$	λ_{abs} (ϵ)	λ_{em} (Φ)	$\Delta\nu$	λ_{abs} (ϵ)	λ_{em} (Φ)	$\Delta\nu$
Methanol (0.309)	417 (2.58)	575 (0.52)	6589	456 (2.04)	663 (<0.01)	6846	391 (1.95)	469 (0.11)	4253	404 (1.08)	596 (0.13)	7169
Ethanol (0.289)	417 (2.08)	564 (0.57)	6250	455 (0.83)	659 (0.016)	6803	391 (2.03)	465 (0.12)	4070	398 (1.08)	586 (0.30)	7234
Acetonitrile (0.305)	398 (1.42)	552 (0.50)	7009	448 (1.67)	668 (0.02)	7351	391 (4.40)	473 (0.06)	4433	398 (1.17)	560 (0.49)	7411
DMSO (0.263)	425 (1.96)	564 (0.60)	5798	461 (2.88)	674 (0.015)	6855	402 (2.10)	503 (0.14)	4994	413 (1.30)	589 (0.26)	6344
Acetone (0.284)	400 (1.58)	542 (0.48)	6549	448 (1.58)	658 (0.06)	7123	392 (3.06)	466 (0.06)	4050	392 (1.15)	554 (0.52)	6975
Chloroform (0.148)	408 (1.65)	521 (0.44)	5315	461 (1.63)	624 (0.36)	5666	387 (1.76)	463 (0.15)	4241	405 (1.29)	543 (0.42)	6354
Ethyl Acetate (0.200)	396 (1.18)	513 (0.41)	5759	446 (1.17)	604 (0.77)	5865	388 (2.81)	453 (0.04)	3698	393 (0.79)	527 (0.39)	6260
THF (0.210)	405 (1.29)	516 (0.55)	5311	450 (1.86)	607 (0.54)	5747	391 (2.45)	451 (0.03)	3402	397 (1.10)	530 (0.57)	6119
Toluene (0.013)	406 (1.33)	487 (0.40)	4096	448 (1.83)	552 (0.81)	4205	387 (2.61)	456 (0.03)	3909	399 (1.30)	506 (0.40)	5617

^a λ_{abs} : absorption maximum; ϵ : molar absorptivity (10^4); λ_{em} : emission maximum; Φ : Quantum yield; $\Delta\nu$: Stokes shift (cm^{-1}); Δf : orientation polarizability of Lippert equation.

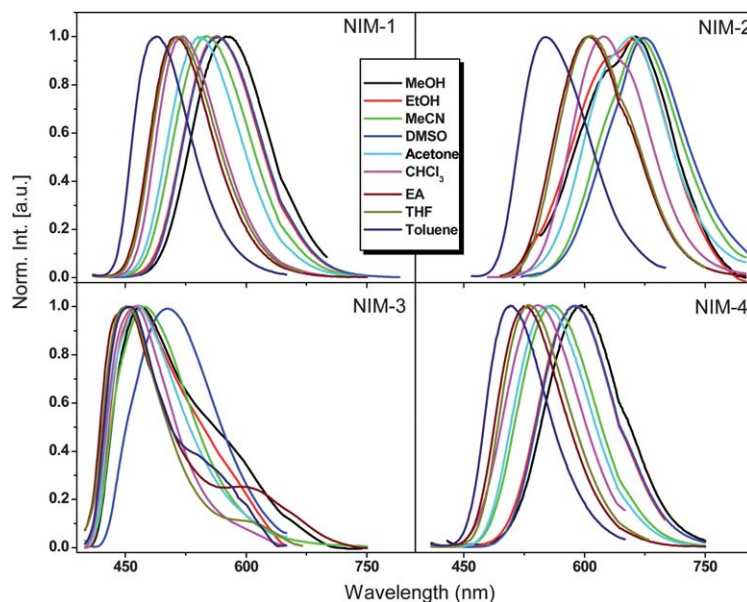


Fig. 1 Normalized fluorescence emission spectra of 20 μM NIM compounds in different solvents. Excited wavelengths are absorption maxima. The emission peaks show red shift with increasing polarity of solvents.

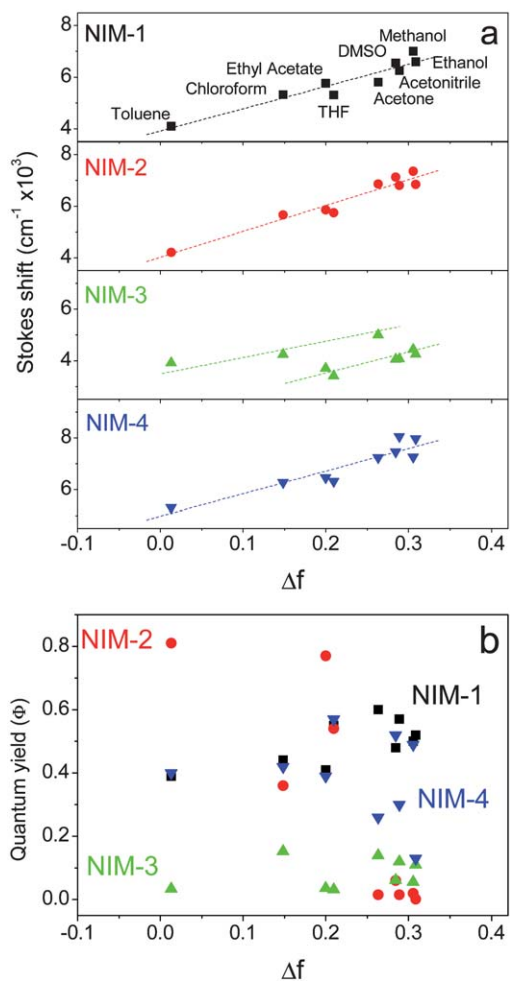


Fig. 2 (a) the Lippert-Mataga plot of the Stokes shift $\Delta\nu$, (b) quantum yields of NIM *versus* the solvent polarity Δf (ϵ , n).

the linear correlation in the polar protic solvents such as ethanol and methanol which can potentially undergo hydrogen bonding interactions with dipolar dyes. We found that the Stokes shift of **NIM-3** was weakly dependent on the polarity with two slopes, but showed an appreciable change in aprotic solvents. Using a value of ~ 7.0 Å for the radius of the Onsager cavity of the naphthalimide derivatives (7.17, 7.89, 7.20 and 7.09 Å for **NIM-1**, **NIM-2**, **NIM-3**, and **NIM-4**, respectively), $\Delta\mu$ values of ~ 16.8 D for **NIM-1**, ~ 20.9 D for **NIM-2**, and ~ 16.5 D for **NIM-4** were obtained from the slopes. However, the $\Delta\mu$ value was relatively smaller in **NIM-3** (~ 11.8 and ~ 15.2 D), which bears an electron withdrawing group, compared to those compounds bearing electron donating groups. The large values of $\Delta\mu$ indicate a substantial contribution of intramolecular charge transfer (ICT) in the excited states of these NIM derivatives. In general, the ICT states of **NIM-1**, **NIM-2**, and **NIM-4** have larger dipole moments in the excited state than in the ground state as a result of the charge separation between the donor and acceptor. Thus, we can support colorful fluorophores based on NIM derivatives which can form an ICT state that is normally sensitive to the solvent polarity.

The fluorescence quantum yields of the **NIM-1**–**NIM-4** dyes showed no direct correlation with the solvent polarity parameters, as shown in Fig. 2b. Compound **NIM-2** produced very high quantum yields (>0.8) under nonpolar solvents while **NIM-3** exhibited low photoluminescence ability (<0.2) in all solvents. The quantum yield values of **NIM-1** and **NIM-4** in the evaluated non-protic solvents were found to be between about 0.4 and 0.6 and their quantum yields also remained high in polar non-protic solvents like acetonitrile. However, in the polar protic methanol and ethanol solutions, the fluorescence emission of the **NIM-2**–**NIM-4** compounds were more strongly quenched, especially in the case of **NIM-2** and **NIM-3** ($\Phi_F < 0.01$), while **NIM-1** was still significantly fluorescent ($\Phi_F \sim 0.52$).

Unique optical properties of NIM derivatives

When compared with other NIM derivatives, compound **NIM-1** exhibited the most stable luminescence properties in most organic solvents, with quantum yields ranging from 0.4 to 0.6 (Table 1 and Fig. 2b). Based on our knowledge, fluorophores

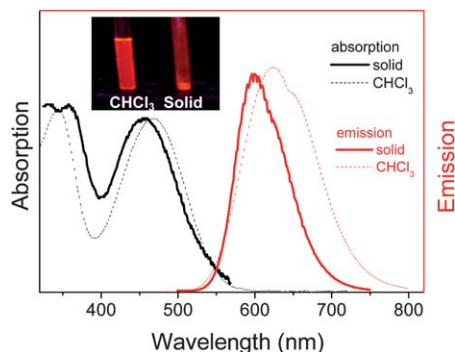


Fig. 3 Normalized absorption, fluorescence spectra and a photo of **NIM-2** in the solid state and in chloroform.

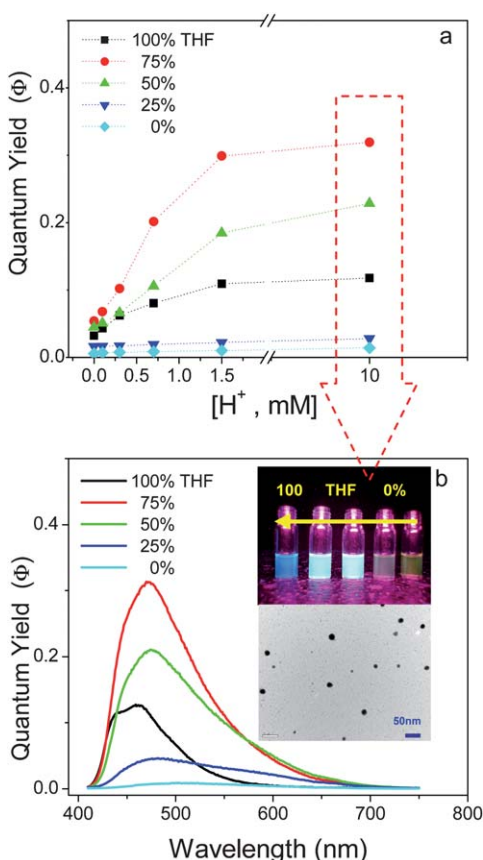


Fig. 4 Illustrations of FONs for **NIM-3**; a) plots of the fluorescent intensities of variable volumes of mixed solutions *versus* concentration of $[H^+]$ values. The preparation of mixed solution was described in ref. 26. b) Emission spectral variations for **NIM-3** under 0, 25, 50, 75 and 100 percentages of 10 mM HCl aqueous solutions mixing ratios with THF. (Excitation wavelength for each solution is 400 nm.) Insets show the photographs and TEM images of nanoparticles obtained under 10 mM HCl aqueous solutions mixed with THF, 25/75 v/v, and scale bar: 50 nm.

that can be successfully applied were based on a single type of fluorophore structure, common to all integrated sensor molecules. The fluorescent optical property of **NIM-1** makes this proposal become possible when we successfully designed and synthesized compound **NIM-4**. Indeed, the phenol moiety can be easily modified or labeled using suitable spacers to become optical sensors, non-doping OLEDs, or laser dyes. Furthermore, we expect that this type of fluorophore will be useful as a cellular probe due to its unique optical property.

On the other hand, as shown in Fig. 3, **NIM-2** showed strong fluorescence in the solid state with an emission maxima at 597 nm (fwhm = 68 nm), which was excitation wavelength independent, and Stokes shift of $\sim 5207\text{ cm}^{-1}$. When compared with the solution spectrum, the narrower solid-state emission band is intriguing because spectral broadening is a very common phenomenon for solid emitting materials. Thus, we propose that there are few intermolecular interactions between molecules, and together with a large Stokes shift, this provides favorable factors that eliminate self-quenching and enhance their solid fluorescence.²⁵ In this case, the introduction of a triphenylamine ring increases the steric hindrance, which prevents the molecules from packing compactly, thereby avoiding the spectral broadening. As discussed above, other molecules of NIM have better planarity and are regularly parallel to each other, with partial π - π stacking over the naphthalimide-styrene core scaffold. Therefore, the large red-shift in the solid emission maximum in **NIM-2** can be attributed to the increased intermolecular interactions in the solid state when compared to those in the solutions. This strong fluorescent emission in its solid state has broadened the family of AIEE fluorophores.

Another phenomenon of AIEE is presented as a form of fluorescent organic nanoparticles. When we studied the emission spectra of compound **NIM-3** under mixing volume ratios of

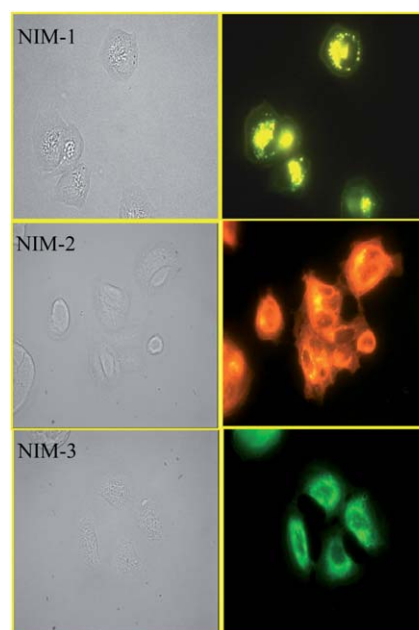


Fig. 5 The bright field image (left) and fluorescence images (right, light path through a 380/10 nm bp filter and emission was collected and filtered through a 450-nm lp filter) of MCF-7 breast cancer cells incubated with 10 μM NIM compounds for 4 h.

solutions containing acidic aqueous and tetrahydrofuran (THF),²⁶ the fluorescence intensities of **NIM-3** showed an interesting change. As shown in Fig. 4, the emission intensity of **NIM-3** increased drastically when $[H^+]$ was added. The quantum yields reached a maximum value in 75% volume fractions of the THF, and the AIEE properties eventually became saturated in the presence of 1.5 mM concentration of acid (Fig. 4a). Under these conditions, the relative TEM images (insets of Fig. 4b) clearly showed nanoparticles that were very fine spheres with a mean diameter of 5–20 nm. Based on previous studies, we considered that protonated **NIM-3** (**NIM-3H⁺**) should serve as a surfactant-like molecule that can further self-assemble to form micelle-like nanoparticles due to its amphiphilic characteristic.¹⁸ Accordingly, a FON model was developed based on water/aprotic solvent pair solutions. Overall, we propose that the **NIM-3H⁺** molecule can aggregate to form micelles and that AIEE phenomenon is the cause of FONs. Alternatively, in neutral water/THF mixed solutions, compounds do not exhibit AIEE under the same experimental conditions. Thus, we conclude that a FONs model which was formed with aggregations of **NIM-3H⁺**, but not **NIM-3**.

Cell staining

Cell permeability allows the compounds to enter living cells enabling intracellular applications. To examine if NIM

derivatives can enter cells and undergo intracellular localization to serve as a fluorescence probe, cells were incubated with NIM derivatives and then subjected to fluorescence microscopy imaging. Fig. 5 showed the fluorescence microscopy cellular images of MCF7 (Human breast adenocarcinoma cell line) treated with **NIM-1**, **NIM-2** and **NIM-3** for 4 h. Surprisingly, fluorescent images were observed in all three compounds with unique bright patterns (threads or bright spots). When we checked their cellular localization, the majority of distribution of **NIM-1** was merged with MitoTracker while that of **NIM-2** was merged with LysoTracker. And the **NIM-3** was partially located in the Endoplasmic Reticulum (ER) and lysosome. (Fig. S, ESI†) However, there is no question that these three compounds can penetrate the cellular membrane and stay in the cytoplasm. Based on our results, the emission abilities of **NIM-2** and **NIM-3** in most solutions were very low. These fluorescent images are worthy of investigation not only to determine the subcellular localizations, but also to resolve the luminance mechanisms.

The cellular staining results of compounds **NIM-1** and **NIM-2** in co-cultured MRC-5 normal lung fibroblast cells and CL1-0 lung cancer cells were further examined by fluorescence confocal microscopy. The molecular imaging of **NIM-1** under confocal microscopy (Fig. 6a–d) and the λ (wavelength) scanning spectra did not differ between cancer and normal cells, and their emission spectra were located in the reasonable range as shown in

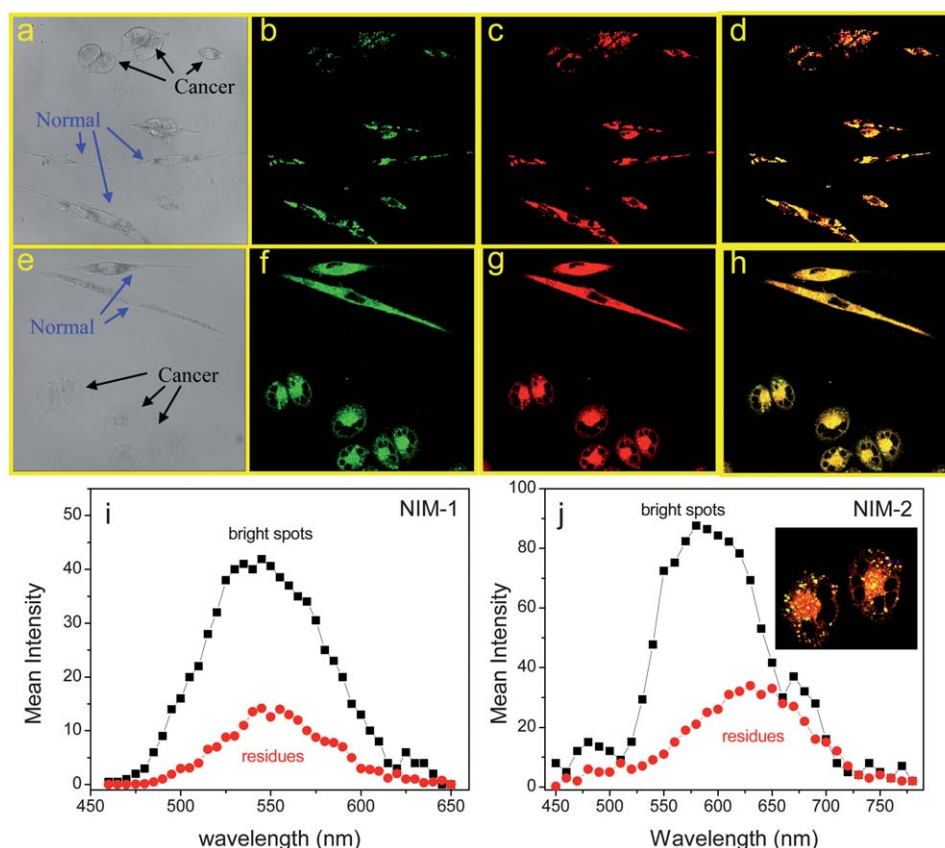


Fig. 6 Confocal microscopy images of co-cultured CL1-0 lung cancer and MRC-5 normal lung fibroblast cell lines. Cells were incubated with 10 μ M compound for 4 h, and a 405 nm diode laser was used as the light source. Compound **NIM-1**: a. Bright field image; b. spectra recorded at 450–560 nm in PMT 1; c. 530–650 nm in PMT 2; d. merger of b with c; i. λ scanning from 460 to 650 nm with 5 nm integration. Compound **NIM-2**: e. Bright field image; f. spectra recorded at 450–590 nm in PMT 1; g. 560–740 nm in PMT 2; h. merger of f with g; j. λ scanning from 450 to 780 nm with 10 nm integration, insert photo represents the zoom in of h but filter cut at 560 nm. The spectra were obtained from the average of 50 individual cancer and normal cells.

Fig. 6i. However, the cellular staining result obtained using **NIM-2** was noteworthy. In contrast to the results observed in normal cells, cancer cells showed bright spots by confocal microscopy (Fig. 6e–h) when the spectra were recorded at 450–590 nm in PMT 1 and 550–740 nm in PMT 2. Additionally, the merge gallery revealed bright spots on cancer cells but not normal cells. Evaluation of the λ scanning spectra suggests a different emission wavelength of **NIM-2** between bright spots (~595 nm) and others cancer cell lines as well as normal cells (Fig. 6j). Similar results were also observed in other cancer cell lines. These results indicate that **NIM-2** molecules generally spread in the cytoplasm of living cells and accumulate in cancer cells, which results in the generation of bright spots. These distinct cellular staining patterns indicate that **NIM-2** can be used to differentiate cancer cells from normal cells once suitable filters (550–620 nm) are constructed—as shown in the inset image in Fig. 6j, in which only cancer cells presented bright spots in the cell staining. Unfortunately, observation of **NIM-3** under confocal microscopy was not successful owing to its higher absorption energy.

Investigation of the brightness of NIM derivatives in cells

Based on the above optical results, the apparent fluorescence emission of **NIM-1** was observed, while **NIM-2** and **NIM-3** possess AIEE properties. It is reasonable that **NIM-1** presents cellular brightness because its emission ability is strong in most of solvents or environments. However, the cellular staining results of compounds **NIM-2** and **NIM-3** are interesting. Indeed, the quantum yields of **NIM-2** and **NIM-3** in most solvents were very low while strong fluorescence only occurred when **NIM-2** dissolved in very low ET30 solvents. Thus, the bright cellular image of **NIM-2** can be explained by two possibilities. First, the cellular environment in which the **NIM-2** molecule was located should have a lower polarity condition. Second, molecules aggregated with very high concentration; that is, molecular imaging of **NIM-2** is the representation of AIEE. Both of these possibilities would result in a strong emission phenomenon of this compound in cells. Moreover, the bright cellular image of **NIM-3** should be attributed to one more possibility; fluorescence enhancement arose from FONs phenomenon under acidic condition. It is known that cellular cytoplasm is acidic and lysosomes maintain at lower pH.²⁷ Therefore, it is possible that neutral **NIM-3** can permeate the cell membrane and be protonated in the cytoplasm to form FONs, and consequently show bright cellular images. From this cursory study, we suggest that both the **NIM-2** and **NIM-3** cases of molecular imaging are due to the presentation of AIEE, but that they function through different mechanisms. Nevertheless, we support colorful cellular probes with similar exciting light sources (under fluorescent microscopy, Fig. 5) for the application of molecular imaging.

Conclusions

The results of this study indicate that colorful fluorophores were developed from NIM derivatives and their large Stokes shifts can prevent self-quenching and measurement errors caused excitation light and scattering. **NIM-1**, **NIM-2**, and **NIM-3** clearly

showed good permeability and were well dispersed in the cytoplasm. First, investigation of **NIM-1** revealed that **NIM-4** may serve as a precursor of DNA or protein labelling markers, for example, conjugate to isothiocyanate and succinimidyl ester functional groups with suitable spacers.²⁸ Second, the weak luminescence of **NIM-2** and **NIM-3** can achieve bright cellular imaging owing to their AIEE properties. More importantly, **NIM-2** can be used in cancer cell recognition. Finally, we have developed color fluorescent probes, with varying emission wavelengths at a fixed excitation wavelength, for application in cellular imaging. Eventually, the fluorescence-environment dependence, large Stokes shift, long emission wavelength, permanent fluorescence quantum yields, and AIEE of these naphthalimide derivatives fluorophores can be used to develop ultrasensitive fluorescent molecular probes to study a variety of biological events and processes.

Acknowledgements

This work was supported financially by the National Science Council (NSC 99-2113-M-005 -011-MY2) of Taiwan.

Notes and references

- (a) K. Hunger, editor. *Industrial dyes: chemistry, properties, application*. Wiley-VCH 2003, pp. 1–12; (b) P. Gregory, *High technology applications of organic colorants*. New York: Plenum 1991.
- A. P. de Silva, H. Q. N. Gunaratne, T. Gunnlaugsson, A. J. M. Huxley, C. P. McCoy, J. T. Rademacher and T. E. Rice, *Chem. Rev.*, 1997, **97**, 1515.
- (a) S. A. Jenekhe and J. A. Osaheni, *Science*, 1994, **265**, 765; (b) R. H. Friend, R. W. Gymer, A. B. Holmes, J. H. Burroughes, R. N. Marks, C. Taliani, D. D. C. Bradley, D. A. Dos Santos, J. L. Brédas, M. Lögdlund and W. R. Salaneck, *Nature*, 1999, **397**, 121; (c) S. J. Toal, K. A. Jones, D. Magde and W. C. Trogler, *J. Am. Chem. Soc.*, 2005, **127**, 11661.
- (a) S. Wang, W. J. Oldham, R. A. Hudack and G. C. Bazan, *J. Am. Chem. Soc.*, 2000, **122**, 5695; (b) L. H. Chan, R. H. Lee, C. F. Hsieh, H. C. Yeh and C. T. Chen, *J. Am. Chem. Soc.*, 2002, **124**, 6469; (c) A. Hagfeldt and M. Grätzel, *Chem. Rev.*, 1995, **95**, 49; (d) J. Y. Kim and F. E. Osterloh, *J. Am. Chem. Soc.*, 2005, **127**, 10152; (e) S. B. Noh, R. H. Kim, W. J. Kim, S. Kim, K. S. Lee, N. S. Cho, H. K. Shim, H. E. Pudavar and P. N. Prasad, *J. Mater. Chem.*, 2010, **20**, 7422.
- (a) G. Yu, S. Yin, Y. Liu, J. Chen, X. Xu, X. Sun, D. Ma, X. Zhan, Q. Peng, Z. Shuai, B. Z. Tang, D. Zhu, W. Fang and Y. Luo, *J. Am. Chem. Soc.*, 2005, **127**, 6335; (b) J. Luo, Z. Xie, J. W. Y. Lam, L. Cheng, H. Chen, C. Qiu, H. S. Kwok, X. Zhan, Y. Liu, D. Zhu and B. Z. Tang, *Chem. Commun.*, 2001, 1740; (c) J. Chen, H. Peng, C. C. W. Law, Y. Dong, J. W. Y. Lam, I. D. Williams and B. Z. Tang, *Macromolecules*, 2003, **36**, 4319; (d) Z. Li, Y. Dong, B. Mi, Y. Tang, M. Hössler, H. Tong, Y. Dong, J. W. Y. Lam, Y. Ren, H. H. Y. Sung, K. S. Wong, P. Gao, I. D. Williams, H. S. Kwok and B. Z. Tang, *J. Phys. Chem. B*, 2005, **109**, 10061.
- (a) B. K. An, S. K. Kwon, S. D. Jung and S. Y. Park, *J. Am. Chem. Soc.*, 2002, **124**, 14410; (b) B. K. An, D. S. Lee, Y. S. Park, H. S. Song and S. Y. Park, *J. Am. Chem. Soc.*, 2004, **126**, 10232; (c) S. J. Lim, B. K. An, S. D. Jung, M. A. Chung and S. Y. Park, *Angew. Chem., Int. Ed.*, 2004, **43**, 6346.
- F. Wang, M. Y. Han, K. Y. Mya, Y. Wang and Y. H. Lai, *J. Am. Chem. Soc.*, 2005, **127**, 10350.
- K. Itami, Y. Ohashi and J. i. Yoshida, *J. Org. Chem.*, 2005, **70**, 2778.
- C. J. Bhongale, C. W. Chang, C. S. Lee, E. W. G. Diao and C. S. Hsu, *J. Phys. Chem. B*, 2005, **109**, 13472.
- (a) H. Görner, S. Khanra, T. Weyhermüller and P. Chaudhuri, *J. Phys. Chem. A*, 2006, **110**, 2587; (b) W. Tang, Y. Xiang and A. Tong, *J. Org. Chem.*, 2009, **74**, 2163.

- 11 (a) T. Martýnski, E. Mykowska and D. Bauman, *J. Mol. Struct.*, 1994, **325**, 161; (b) T. Martýnski, A. Mykowska, R. Stolarski and D. Bauman, *Dyes Pigm.*, 1994, **25**, 115.
- 12 (a) I. Grabtchev, T. Philipova, P. Meallier and S. Guittonneau, *Dyes Pigm.*, 1996, **31**, 31; (b) I. Grabchev and T. Konstantinova, *Dyes Pigm.*, 1997, **33**, 197; (c) A. Dorlars, W. C-Schellhammer and J. Schroeder, *Angew. Chem., Int. Ed. Engl.*, 1975, **14**, 665.
- 13 (a) W. Adam, X. Qian and C. Saha-Moller, *Tetrahedron*, 1993, **49**, 417; (b) X. Qian, J. Tang, J. Zhang and J. Zhang, *Dyes Pigm.*, 1994, **25**, 109.
- 14 Z.-F. Tao, X. Qian and J. Tang, *Dyes Pigm.*, 1996, **30**, 247.
- 15 (a) J. Wang and X. Qian, *Chem. Commun.*, 2006, **42**, 109; (b) X. Guo, X. Qian and L. Jia, *J. Am. Chem. Soc.*, 2004, **126**, 2272; (c) R. Parkesh, T. C. Lee and T. Gunnlaugsson, *Org. Biomol. Chem.*, 2007, **5**, 310.
- 16 (a) C.-G. Niu, G.-M. Zeng, L.-X. Chen, G.-L. Shena and R.-Q. Yu, *Analyst*, 2004, **129**, 20; (b) D. Cui, X. Qian, F. Liu and R. Zhang, *Org. Lett.*, 2004, **6**, 2757; (c) T. Sabine, H. Patrick, H. Thomas and J. M. Gerhard, *Org. Biomol. Chem.*, 2008, **6**, 4319.
- 17 S. Y. Su, H. H. Lin and C. C. Chang, *J. Mater. Chem.*, 2010, **20**, 8653–8658.
- 18 H. H. Lin, S. Y. Su and C. C. Chang, *Org. Biomol. Chem.*, 2009, **7**, 2036.
- 19 L. F. Vieira Ferreira and S. M. B. Costab, *J. Lumin.*, 1991, **48–49**, 395.
- 20 C. C. Chang, S. H. Kuo, C. C. Kang and T. C. Chang, *J. Lumin.*, 2006, **119–120**, 84.
- 21 (a) C. C. Chang, K. J. Chen and L. J. Yu, *J. Org. Chem.*, 1999, **64**, 5603; (b) C. C. Chang, Y. J. Wu and T. C. Chang, *J. Chin. Chem. Soc.*, 2003, **50**, 185.
- 22 (a) P. Yang, Q. Yang and X. Qian, *Tetrahedron*, 2005, **61**, 11895; (b) G. R. Bardajee, A. Y. Li, J. C. Haley and M. A. Winnik, *Dyes Pigm.*, 2008, **79**, 24.
- 23 (a) P. R. Bangal, S. Panja and S. Chakravorti, *J. Photochem. Photobiol., A*, 2001, **139**, 5; (b) R. O. Loutfy and B. A. Arnold, *J. Phys. Chem.*, 1982, **86**, 4205.
- 24 (a) K. Rotkiewicz, K. H. Grellman and Z. R. Grabowski, *Chem. Phys. Lett.*, 1973, **19**, 315; (b) W. Rettig, *Angew. Chem., Int. Ed. Engl.*, 1986, **25**, 971; (c) A. Nag and K. Bhattacharyya, *Chem. Phys. Lett.*, 1990, **169**, 12.
- 25 Y. Zhou, Y. Xiao, S. Chi and X. Qian, *Org. Lett.*, 2008, **10**, 633.
- 26 Preparation of mixed solutions: First, the 0 to 10 mM of HCl aqueous solutions were prepared; and then these acidic solutions were directly mixed with THF with volume ratios of 0, 25, 50, 75, and 100 percent. While the acidic THF solution (as we assign acidic aqueous/THF = 0/100 v/v) is achieved by adding an equal volume of 12 M HCl as to prepare the 0 to 10 mM of HCl aqueous solutions.
- 27 I. Kazuhiro, A. Takafumi and G. Hidemi, *BioTechniques*, 2008, **45**, 465.
- 28 J. H. Flanagan, S. H. Khan, S. Menchen, S. A. Soper and R. P. Hammer, *Bioconjugate Chem.*, 1997, **8**, 751.